

Quantifying Tripartite Spatial and Energy-Time Entanglement in Nonlinear Optics

James Schneeloch,^{1,*} Richard J. Birrittella,¹ Christopher C. Tison,¹

Gregory A. Howland,^{2,3} Michael L. Fanto,¹ and Paul M. Alsing¹

¹*Air Force Research Laboratory, Information Directorate, Rome, New York, 13441, USA*

²*Microsystems Engineering, Rochester Institute of Technology, Rochester, New York 14623, USA*

³*School of Physics and Astronomy, Rochester Institute of Technology, Rochester, New York 14623, USA*

(Dated: October 14, 2021)

In this work, we provide a means to quantify genuine tripartite entanglement in arbitrary (pure and mixed) continuous-variable states as measured by the Tripartite Entanglement of formation — a resource-based measure quantifying genuine multi-partite entanglement in units of elementary Greenberger-Horne-Zeilinger (GHZ) states called gebits. Furthermore, we predict its effectiveness in quantifying the tripartite spatial and energy-time entanglement in photon triplets generated in cascaded spontaneous parametric down-conversion (SPDC), and find that ordinary nonlinear optics can be a substantial resource of tripartite entanglement.

I. INTRODUCTION

As quantum networking and computing platforms grow more sophisticated, it is more important than ever to develop means of efficiently characterizing the quantum resources present. To that end, many advances have been made over the last few years in quantifying the entanglement present between two groups of increasingly high-dimensional systems [1, 2]. However, when it comes to quantifying *multi-partite* entanglement in high-dimensional systems, the field remains relatively underdeveloped with notable exceptions [3, 4] using generalizations of the three-tangle [5], a monotone based on the residual entanglement [6], which identifies most but not all tripartite entangled states. Recently, resource-based entanglement measures that both faithfully identify all multi-partite entangled states, and are additive over copies of the state to be measured have been developed [7, 8], but the fundamental challenge of efficiently quantifying genuine multi-partite entanglement in high-dimensional systems remains to be answered [9].

As experimental sources of entanglement have a finite preparation uncertainty, strategies toward quantifying multi-partite entanglement must be applicable to mixed as well as pure states. To that end, there do exist multiple witnesses of genuine continuous-variable tripartite entanglement that apply to arbitrary quantum states [10–14], which have been used successfully in experiment [15]. In general, witnesses of genuine tripartite entanglement date back as early as 1987 [16], but quantifying more than a nonzero amount of tripartite entanglement present has remained elusive.

Within the last year, the challenge of quantifying genuine tripartite entanglement in mixed states has been answered in part in [17], where correlations between observables of qudits were used to place a lower bound on the tripartite entanglement of formation E_{3F} — a measure of genuine tripartite entanglement that compares the

arbitrary state being measured to a comparable number of three-qubit GHZ states, known as three-party gebits. This strategy to quantify genuine tripartite entanglement was explicitly dependent on the dimension d of the quantum systems, so that adapting it for continuous-variable degrees of freedom remained an open challenge [18]. In this work, we present a strategy to quantify genuine tripartite entanglement of arbitrary (pure and mixed-state) continuous-variable systems using the correlations naturally present in many of these systems. In particular, we examine the tri-partite spatial and energy-time entanglement present in cascaded $\chi^{(2)}$ spontaneous parametric down-conversion (SPDC), in which one pump photon is split into two daughter photons, followed by one daughter photon down-converting into two granddaughter photons. The spatial correlations in this system are qualitatively identical to those in $\chi^{(3)}$ SPDC (a single-step photon triplet generation process in nonlinear optics), and generation rates are comparable with one another [19–22], but we focus on cascaded SPDC, as this process is more well-studied [23].

II. FOUNDATIONS AND MOTIVATION: QUANTIFYING GENUINE TRIPARTITE CONTINUOUS-VARIABLE ENTANGLEMENT

Entanglement is defined with respect to separability. Any quantum state $\hat{\rho}$ of three parties A , B , and C , that factors out into a product of states for each party, or any mixture of such factorable states is defined to be separable:

$$\hat{\rho}_{ABC}^{(sep)} = \sum_i p_i (\hat{\rho}_{Ai} \otimes \hat{\rho}_{Bi} \otimes \hat{\rho}_{Ci}) \quad (1)$$

All other states are entangled.

With more than two parties, there are multiple forms of separability, defining multiple forms of entanglement. For example, states of the form $A \otimes BC$:

$$\hat{\rho}_{A \otimes BC} = \sum_i p_i (\hat{\rho}_{Ai} \otimes \hat{\rho}_{BCi}) \quad (2)$$

* james.schneeloch.1@us.af.mil

are known as biseparable because they can be expressed as mixtures of states that factor out as a product of two terms — in this case, one for A and another for the joint state of BC . To demonstrate tri-partite entanglement, the state must at least be in no way biseparable, but there is more to it. Proving ABC is genuinely tripartite entangled requires showing not just that the state is outside all three classes of biseparable states (i.e., $A \otimes BC$, $B \otimes AC$ and $C \otimes AB$), but that the state cannot be made out of any arbitrary mixture of states coming from one or more of these classes. This distinction is important because it is possible to combine biseparable states from multiple classes to obtain mixed states that are outside all of these sets. Such fully inseparable states are not genuinely tripartite entangled.

The measure of genuine tripartite entanglement we will be using in this paper is the tripartite entanglement of formation E_{3F} , which for parties A , B , and C , is given by:

$$E_{3F}(ABC) = \min_{|\psi\rangle_i} \sum_i p_i \min\{S_i(A), S_i(B), S_i(C)\} \quad (3)$$

where the first minimum is taken over all pure state decompositions of $\hat{\rho}_{ABC}$ and the second minimum is of the entanglement entropy over all bipartitions of each constituent pure state in the decomposition. This measure, first discussed in [7], is a generalization of the regular entanglement of formation, and is: (1) greater than zero if and only if the state is genuinely tripartite entangled; (2) invariant under local unitary transformations; (3) monotonically decreasing under local operations and classical communication (LOCC), and (4) additive over tensor products, so that m copies of a given entangled state will have m times the value of E_{3F} that one copy does. This facilitates side-by-side comparisons of multiple low-dimensional entangled states with fewer high-dimensional entangled states. For pure tripartite states, E_{3F} is simply equal to the minimal entropy between subsystems A , B , and C . In [17], we were able to lower-bound E_{3F} using correlations between observables of d -dimensional systems, but in this article, we show how one can also do this for continuous-variable (high-dimensional) systems.

To witness genuine tripartite entanglement in both pure and mixed states, one can start with a convex witness of genuine tripartite entanglement for pure states. Here, the convex witness is any convex function f of the quantum state $|\psi\rangle_{ABC}$ such that for some value η , $f > \eta$ witnesses genuine tripartite entanglement. The convexity allows us to immediately apply these witnesses to mixed states because the average value of a convex function cannot increase under mixing.

Once a convex witness of genuine tripartite entanglement for pure states is found, it is readily adapted to fully general (i.e., mixed) states. Given f is convex, if $\hat{\rho}$ has a pure state decomposition:

$$\hat{\rho} = \sum_i p_i |\psi_i\rangle\langle\psi_i|, \quad (4)$$

the witness will obey the inequality:

$$f(\hat{\rho}) \leq \sum_i p_i f(|\psi_i\rangle\langle\psi_i|) \quad (5)$$

Since $f > \eta$ witnesses genuine tripartite entanglement in a pure state, it must also follow that for any mixture of pure states $\hat{\rho}$, that $f(\hat{\rho}) > \eta$ witnesses genuine tripartite entanglement as well. This forces at least one element in any pure state decomposition of $\hat{\rho}$ to be genuinely tripartite entangled, which is sufficient to prove genuine tripartite entanglement in the mixed state case. This general strategy of constructing convex witnesses for pure states has been used to great success to construct multi-partite entanglement witnesses from uncertainty relations in [11].

To *quantify* genuine tripartite entanglement, we use convex entanglement witnesses that bound the quantum conditional entropy. In particular, we found in [24], that for Fourier-conjugate position x and momentum $k = p/\hbar$:

$$\log(2\pi) - h(x_A|x_B, x_C) - h(k_A|k_B, k_C) \leq -S(A|BC) \quad (6a)$$

$$\log(2\pi) - h(x_B|x_C, x_A) - h(k_B|k_C, k_A) \leq -S(B|CA) \quad (6b)$$

$$\log(2\pi) - h(x_C|x_A, x_B) - h(k_C|k_A, k_B) \leq -S(C|AB) \quad (6c)$$

Here, $h(x_A|x_B, x_C) = h(x_A, x_B, x_C) - h(x_B, x_C)$, and $h(x_A, x_B, x_C)$ is the continuous Shannon entropy [25] of the joint probability density of x_A , x_B , and x_C . In addition, $S(A|BC) = S(ABC) - S(BC)$ is the quantum conditional entropy where for example, $S(ABC)$ is the von Neumann entropy of density matrix $\hat{\rho}_{ABC}$. The left hand sides of (6) witness entanglement in their respective bipartitions when they are greater than zero. All logarithms are taken to be base two, since we measure entropy in bits.

With the preceding three relations (6), we find functions of x and k that bound the left hand side of all three at once. For momentum k , we have for the entropy of the sum of the three momenta:

$$h(k_A + k_B + k_C) \geq \begin{cases} h(k_A|k_B, k_C) \\ h(k_B|k_A, k_C) \\ h(k_C|k_A, k_B) \end{cases} \quad (7)$$

and for position, we have for the entropy of the mean difference between positions:

$$h\left(x_A - \frac{x_B + x_C}{2}\right) \geq \begin{cases} h(x_A|x_B, x_C) - \log(2) \\ h(x_B|x_A, x_C) - \log(2) \\ h(x_C|x_A, x_B) - \log(2) \end{cases} \quad (8)$$

See proof in Appendix A. Together, these allow us to consolidate these separate bounds into one:

$$\begin{aligned} & h\left(x_A - \frac{x_B + x_C}{2}\right) + h(k_A + k_B + k_C) \\ & \geq \log(\pi) + \max\{S(A|BC), S(B|AC), S(C|AB)\} \quad (9) \end{aligned}$$

To obtain a bound for the tripartite entanglement of formation for pure states, we use the relation for pure states that $-S(A|BC) = S(A)$, and re-arrange the previous inequality to obtain:

$$\min\{S(A), S(B), S(C)\} \geq \log(\pi) - h\left(x_A - \frac{x_B + x_C}{2}\right) - h(k_A + k_B + k_C) \quad (10)$$

This relation is true for every element in the pure state decomposition of $\hat{\rho}_{ABC}$, and therefore for any mixture. Then, because this relation must hold, even if we choose the pure state decomposition that minimizes the left hand side of this relation, we have our bound for the tripartite entanglement of formation E_{3F} :

$$E_{3F}(ABC) \geq \log(\pi) - h\left(x_A - \frac{x_B + x_C}{2}\right) - h(k_A + k_B + k_C) \quad (11)$$

With this bound, we can place a conservative lower limit to E_{3F} on continuous-variable systems where direct calculation is generally intractable even with full knowledge of the state. Moreover, this relation can be adapted into one using standard deviations σ or variances σ^2 instead of entropies (as was accomplished previously for bipartite entanglement in [24]), because the Gaussian distribution is the maximum entropy distribution for a fixed variance:

$$E_{3F}(ABC) \geq -\log\left(2e\sigma\left(x_A - \frac{x_B + x_C}{2}\right)\sigma(k_A + k_B + k_C)\right) \quad (12)$$

Resource measures of multi-partite entanglement are still relatively underdeveloped, but we expect that tools such as these will spur new growth in the field.

1. Generality of application

Although we derived our tripartite entanglement bound (11) using Fourier-conjugate position x and momentum $k = p/\hbar$, any pair of Fourier-conjugate variables will apply, including time t and (angular) frequency ω , or functions of conjugate field quadratures in quantum optics as studied in [26, 27].

Indeed, in [15], Shalm *et al* demonstrated tri-partite energy-time entanglement between photon triplets generated in cascaded SPDC, subject to the assumption that $\sigma(\omega_1 + \omega_2 + \omega_3) = \sigma(\omega_p)$. Their source generates photon triplet detection events at a rate of approximately seven per hour of the course of three days, but using their maximum time uncertainty $\sigma(t_2 - t_1) = 3.7 \times 10^{-10}$ s as an approximation toward the uncertainty $\sigma(t_A - \frac{t_B + t_C}{2})$, and their pump uncertainty $\sigma(\omega_p) = 3.77 \times 10^7$ /s, one could verify as much as 3.72 gubits of tripartite energy-time entanglement, which is already more entanglement than an 11-qubit or 2200-dimensional state can support.

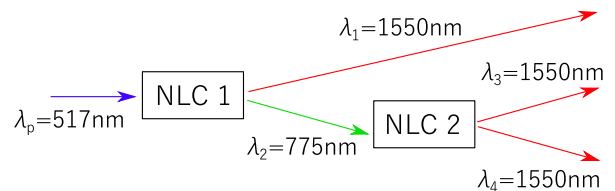


FIG. 1: Basic diagram of degenerate-cascaded SPDC using 517nm pump light to produce triplets at 1550nm. First, light at λ_p is split into wavelengths λ_1 and λ_2 . The light at λ_2 is then split into light at λ_3 and λ_4 .

III. EFFECTIVENESS IN CASCADED SPDC

Having developed our quantitative bound for tripartite entanglement, we now test its effectiveness for a realistic source of tripartite entanglement. In this work, we consider a source of spatially entangled photon triplets generated in degenerate cascaded spontaneous parametric down-conversion (See Fig. 1 for basic diagram). The source would be a pump laser at frequency ω_p interacting with two $\chi^{(2)}$ -nonlinear crystal of length L_z . The first crystal would be phase-matched to produce signal/idler photon pairs at frequencies $2\omega_p/3$ and $\omega_p/3$, respectively. The signal photons would then be directed toward the second crystal chosen to be phase matched for degenerate SPDC taking idler photons at $2\omega_p/3$ and producing photon pairs at $\omega_p/3$.

As shown in Appendix B, the transverse spatial triphoton amplitude of the triplets generated in this process is of the form:

$$\psi(\vec{q}_1, \vec{q}_3, \vec{q}_4) = \mathcal{N}\alpha_p(\vec{q}_1 + \vec{q}_3 + \vec{q}_4)\text{sinc}\left(\frac{\Delta k_z L_z}{2}\right) \quad (13)$$

where here:

$$\Delta k_z = k_{1z} + k_{3z} + k_{4z} - k_{pz} - k_{\Lambda_1} - k_{\Lambda_2} \quad (14)$$

and α_p is the transverse momentum amplitude of the pump field where \vec{q}_p is set equal to $(\vec{q}_1 + \vec{q}_3 + \vec{q}_4)$ by momentum conservation. To clarify: \vec{q} is the projection of momentum \vec{k} onto the transverse plane; k_{1z} is the longitudinal component of the momentum of the lower energy idler photons exiting the first crystal; k_{3z} and k_{4z} are the corresponding momentum components of the photons created in the second crystal; and k_{Λ_1} and k_{Λ_2} are the poling momenta of the first and second crystals. If no periodic poling or quasi-phase matching is employed to achieve these processes, then $(k_{\Lambda_1} = k_{\Lambda_2} = 0)$.

To express the triphoton amplitude purely in terms of transverse momentum components, we use the assumption that this process is collinear to set the sum of the transverse momenta equal to zero, and use trigonometric identities as well as the small-angle approximation to express the individual transverse momenta in terms of the total momentum offset Δk_z :

$$\Delta k_z \approx \frac{3}{2|k_p|} (|\vec{q}_1 + \vec{q}_3|^2 + |\vec{q}_1 + \vec{q}_4|^2 + |\vec{q}_3 + \vec{q}_4|^2) \quad (15)$$

where we assume $|k_1| = |k_3| = |k_4| = (k_{\bar{p}})/3$ for simplicity, where $k_{\bar{p}} = k_p + k_{\Lambda_1} + k_{\Lambda_2}$.

To simplify notation, we will let k_1 refer to the first transverse component of \vec{k}_1 , and define k_3 and k_4 similarly. Since for small arguments of the Sinc function, $\text{sinc}(x^2 + y^2) \approx \text{sinc}(x^2)\text{sinc}(y^2)$, we have as our model for the triphoton wavefunction (for one spatial component):

$$\psi(k_1, k_3, k_4) \approx \mathcal{N} \alpha_p (k_1 + k_3 + k_4) \times \text{sinc} \left(\frac{3L_z}{4k_{\bar{p}}} ((k_3 + k_4)^2 + (k_1 + k_3)^2 + (k_1 + k_4)^2) \right) \quad (16)$$

This function is symmetric under permutations of k_1 , k_3 and k_4 . Moreover, the argument of the sinc function is a quadratic form, so we can simplify it dramatically by transforming to a new basis of coordinates. Taking this, together with the Gaussian approximation of the sinc function in [28], we obtain a simple triple-Gaussian wavefunction for the photon triplets:

$$\psi(k_u, k_v, k_w) = \mathcal{N} e^{-\left(\frac{32a}{9} + 3\sigma_p^2\right)k_u^2} e^{-\frac{8a}{9}k_v^2} e^{-\frac{8a}{9}k_w^2} \quad (17)$$

such that $a = \frac{3L_z}{4k_{\bar{p}}}$, and:

$$k_u = \frac{1}{\sqrt{3}}(k_1 + k_3 + k_4) \quad (18)$$

$$k_v = \frac{2}{\sqrt{6}} \left(-k_1 + \frac{k_3 + k_4}{2} \right) \quad (19)$$

$$k_w = \frac{1}{\sqrt{2}}(k_3 - k_4) \quad (20)$$

and σ_p is the ordinary pump beam radius (i.e., one quarter of the $1/e^2$ beam diameter). Remarkably, our tripartite entanglement bound can also be expressed in terms of these rotated coordinates:

$$E_{3F}(ABC) \geq \log(\pi) - h \left(\frac{\sqrt{6}}{2} x_v \right) - h \left(k_u \sqrt{3} \right) \quad (21)$$

which is further simplified by virtue of its being a Gaussian distribution to:

$$E_{3F}(ABC) \geq -\log(3\sqrt{2}e) - \frac{1}{2} \log(\sigma_{k_u}^2 \sigma_{x_v}^2) \quad (22)$$

with variances:

$$\sigma_{k_u}^2 = \frac{1}{4 \left(\frac{32a}{9} + 3\sigma_p^2 \right)} \quad : \quad \sigma_{x_v}^2 = \frac{8a}{9} \quad (23)$$

and we obtain the final result:

$$E_{3F}(ABC) \geq \frac{1}{2} \log \left(16 + \frac{18\sigma_p^2 k_{\bar{p}}}{L_z} \right) - \log(3\sqrt{2}e). \quad (24)$$

E_{3F} minimum in gebits

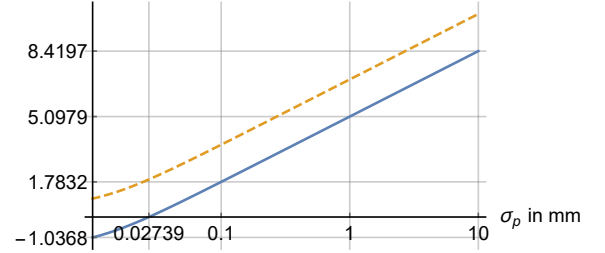


FIG. 2: Plot of the lower limit to E_{3F} in our considered experimental setup of a pair of PPLN crystals of length $L_z = 3\text{mm}$, as a function of the pump beam radius σ_p in millimeters. The lower blue curve gives the amount of tripartite entanglement witnessed by our correlation techniques. The upper dashed yellow curve gives the exact value for E_{3F} for the triple-Gaussian wavefunction. In the limit of high correlation, the difference between these two curves rapidly approaches a constant of $2 \log_2(e) - 1$ or about 1.88 gebits.

A. Predicted tripartite entanglement for reasonable experimental parameters

Let us consider two crystals of periodically poled lithium niobate PPLN whose poling is chosen to be phase matched to the appropriate down-conversion process. At the pump wavelength of 516.67nm, the index of refraction n_p is approximately 2.240, and the poling periods will have to be about $8.84\mu\text{m}$ and $18.99\mu\text{m}$ for each crystal, respectively. From this, the effective pump momentum $k_{\bar{p}}$ is approximately $2.60 \times 10^7/m$. Bulk crystals come in a variety of lengths, but let us assume $L_z = 3\text{mm}$. The only remaining parameter to fix is the Gaussian beam radius σ_p .

In Fig. 2, we have plotted our lower bound for E_{3F} as a function of σ_p and find that this source has potentially a substantial amount of entanglement. In particular, we find for these experimental parameters that a modest beam radius of 1 mm will generate in excess of five gebits of tripartite entanglement in each transverse dimension, giving us in excess of 10 gebits in total. As a basis of comparison, ten gebits of tripartite entanglement is the maximum amount of tripartite entanglement that a 30-qubit or billion-dimensional state can support!

In order to gauge the effectiveness of our technique at quantifying tripartite entanglement, we need to compare the entanglement we can quantify to the total entanglement present in the triple-Gaussian state. Luckily, the triple-Gaussian wavefunction is simple enough to find its Schmidt decomposition using properties of the Double-gaussian wavefunction [29] (see Appendix C for details). For both the double-Gaussian wavefunction of two parties, and the triple-Gaussian wavefunction of three parties, the reduced density operator $\hat{\rho}_A$ has an identical form. The marginal eigenvalues of $\hat{\rho}_A$ are then determined, and from them, the von Neu-

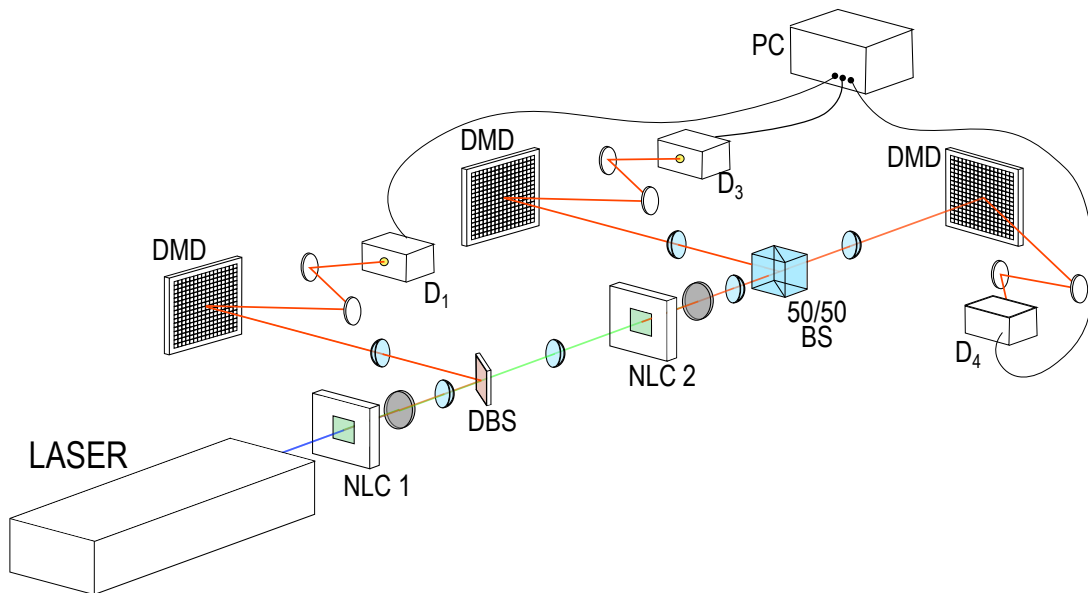


FIG. 3: Diagram of considered experimental setup to measure position correlations between photon triplets generated in cascaded SPDC. Lenses (in blue) are used both to image the plane of the first nonlinear crystal NLC1 onto a digital micromirror device (DMD) and the plane of the second nonlinear crystal (NLC2), and to image the plane of NLC2 onto the final pair of DMD arrays. The three detectors D_1 , D_3 and D_4 are connected to a photon correlator (PC) to record triplet coincidence count rates for each setting of the three DMD arrays, and from this build the joint position probability distribution of the photon triplets from which correlations are obtained.

mann entropy $S(A)$ as well. Finally, because the triple-Gaussian wavefunction corresponds to a pure state, and because it is symmetric under permutations of parties, the exact tripartite entanglement of formation is given as $E_{3F}(ABC) = S(A)$, the von Neumann entropy of system A . In Fig. 2, we plot both the exact value for E_{3F} for the triple-Gaussian wavefunction along with our lower bound to it (24) based on measured correlations (11), and find the gap between the witnessed and total tripartite entanglement rapidly approaches a constant of about 1.88 qubits in the limit of high correlation.

As the pump beam radius σ_p grows wider (alternatively σ_{xu}), the corresponding uncertainty in the transverse momentum σ_{ku} grows smaller while the other principal variances σ_{kv} and σ_{kw} remain constant. This results in the momentum distribution becoming more correlated to a flat plane, and the position distribution more correlated to a single line. That both the position and momentum distributions for three particles would be strongly correlated to single lines is actually forbidden by the uncertainty principle [17], a surprising result since this restriction on correlations does not exist between two particles. Even so, the tripartite correlations discussed in this proposed experiment are optimal in that they approach a continuous-variable analogue of the GHZ state.

B. Considered Experimental Setup

In [2], we showed how one can use a simple experimental setup along with techniques in information theory to adaptively sample the transverse position and transverse momentum correlations in such a way that a very small number of measurements (relative to the state space) can faithfully extract those correlations without overestimating the entanglement present. In this subsection, we discuss how to do the same for the tripartite entanglement generated in our considered setup, referring to Fig. 3 for details.

To begin with, we consider a 517 nm pump laser incident on a nonlinear crystal (labeled NLC 1) quasi-phase-matched for type-I collinear nondegenerate SPDC with signal light centered at $\lambda_1 = 775$ nm and idler light centered at $\lambda_2 = 1550$ nm, respectively. After passing through a pump removal filter, the light would be split by a dichroic beamsplitter (labeled DBS) that transmits 775nm light and reflects 1550nm light. The length of the reflected 1550nm path following the DBS would terminate with a digital micromirror device (DMD) array whose pixels are computer-controlled to reflect the down-converted light toward or away from a photon-counting detector. This arm would be fitted with optics to either image the plane of NLC 1, or its Fourier transform, giving us access to either the position or momentum statistics of that idler photon, respectively. The transmitted arm following the DBS would terminate with the second crystal (labeled NLC 2), and be fitted with 4F imaging optics to

preserve the amplitude and phase of the signal photon.

Next, the signal light at $\lambda_2 = 775\text{nm}$ would pass through the second nonlinear crystal phase-matched and periodically poled for type-0 degenerate collinear SPDC from 775 nm to two sub-idlers centered at $\lambda_3 = \lambda_4 = 1550$ nm. Following NLC2, the residual 775 nm light would be filtered out, and the 1550 nm photon pairs would be split by a 50/50 beamsplitter. Each arm of this wing of the experiment would terminate in a DMD array with optics to image either the field at the plane at NLC 2 onto them, or to image its Fourier transform, thus allowing us access to the position and momentum statistics of this pair as well.

By connecting all three photon detectors to a multi-channel photon correlator (PC), we can record the triplet photon coincidences that occur. By correlating the triplet coincidence count rate to the settings on each DMD array, we can build up a tri-partite joint probability distribution for the positions or the momenta of the photon triplets.

If we were to build up the joint position and momentum statistics one pixel triplet at a time, acquiring the entire distribution at decent resolution would rapidly become intractable. Indeed, current triplet generation rates are improving for both $\chi^{(2)}$ and $\chi^{(3)}$ processes [21, 22, 30], but still are well below one triplet per second per mW of pump power. However, using multi-resolution sampling techniques employed in [2] can solve this scaling issue as more efficient sources of entangled photon triplets continue to be developed. By sampling first at the lowest possible resolution (i.e., $2 \times 2 \times 2$), and next subsampling only in regions with a significant triplet coincidence rate, and iteratively subsampling in the brightest areas of those sub-regions, one can obtain a coarse-grained approximation to these distributions that will never overestimate the entanglement present, and requires a minuscule fraction of the total number of measurements that would be required otherwise. Indeed, in [2], these multi-resolution techniques improved the required acquisition time by at least a factor of 10^7 , and this advantage will only be more dramatic in the tripartite case, due to the higher dimensional space in which these sparse correlations reside.

IV. DISCUSSION: RESOURCE MEASURE CHALLENGES AND FUTURE APPLICATIONS

The major issue with generating tripartite spatial entanglement via cascaded SPDC is dealing with a low generation rate. Even with an optimistic free-space generation rate of 10^8 photon pairs per second per mW of pump power, this implies about 1 in 2.9×10^7 pump photons get converted in each crystal, so that only about 1 in 1.5×10^{15} pump photons end up yielding triplets. For 1 mW of pump power at 517 nm, this would imply a total generation rate of about 2.6 triplets per second. Incorporating reasonable sources of loss reduces this rate by an order of magnitude, which puts it on par with the recent demonstration of a triplet generation rate of 12.4 triplets per minute [30]. Even with the highly efficient structured sensing approach discussed here and in [2], the total acquisition time required would make acquiring these spatial correlations at high resolution and statistical significance beyond current capabilities. However, with the recent advent of spatially-resolving photon detectors (e.g., SPAD arrays), demonstrating tripartite spatial entanglement, even at these low intensities becomes possible. With SPAD arrays one can acquire the maximum information from every photon triplet since the position that they strike each detector would be immediately stored, and a usable tripartite position probability distribution can be acquired with a comparably small number of photons.

porating reasonable sources of loss reduces this rate by an order of magnitude, which puts it on par with the recent demonstration of a triplet generation rate of 12.4 triplets per minute [30]. Even with the highly efficient structured sensing approach discussed here and in [2], the total acquisition time required would make acquiring these spatial correlations at high resolution and statistical significance beyond current capabilities. However, with the recent advent of spatially-resolving photon detectors (e.g., SPAD arrays), demonstrating tripartite spatial entanglement, even at these low intensities becomes possible. With SPAD arrays one can acquire the maximum information from every photon triplet since the position that they strike each detector would be immediately stored, and a usable tripartite position probability distribution can be acquired with a comparably small number of photons.

V. CONCLUSION

The utilization and characterization of multi-partite entanglement is rapidly developing, even while fundamental questions remain to be answered. Here we have presented the first (to our knowledge) technique to quantify genuine tripartite entanglement in continuous-variable systems without the restriction to pure states, enabling us to employ these techniques experimentally. Moreover, we explore a natural source of these tripartite correlations in cascaded spontaneous parametric down-conversion, and find that for reasonable experimental parameters, there is already more tripartite entanglement present than 2-3 dozen qubits can support. On top of this, we were able to gauge the effectiveness of our technique because the high symmetry of the triple-Gaussian wavefunction allowed an explicit calculation of its tripartite entanglement of formation. With current sources of high-dimensional tripartite entanglement owing their strength to the correlations arising from conserved quantities in their interaction, measurement techniques capitalizing on those correlations are highly efficient. Moreover, using entropy-based tools will allow us to efficiently acquire these correlations at variable resolution without ever over-estimating the entanglement present, as was accomplished for two-party entanglement in [2].

ACKNOWLEDGMENTS

We gratefully acknowledge support from the Air Force Office of Scientific Research LRIR 18RICOR028, as well as insightful discussions with Dr. A. Matthew Smith, and Dr. H Shelton Jacinto. Any opinions, findings and conclusions or recommendations expressed in this material are those of the author(s) and do not necessarily reflect the views of AFRL.

- [1] A. Martin, T. Guerreiro, A. Tiranov, S. Designolle, F. Fröwis, N. Brunner, M. Huber, and N. Gisin, Quantifying photonic high-dimensional entanglement, *Phys. Rev. Lett.* **118**, 110501 (2017).
- [2] J. Schneeloch, C. C. Tison, M. L. Fanto, P. M. Alsing, and G. A. Howland, Quantifying entanglement in a 68-billion-dimensional quantum state space, *Nat. Commun.* **10** (2019).
- [3] G. Adesso and F. Illuminati, Continuous variable tangle, monogamy inequality, and entanglement sharing in gaussian states of continuous variable systems, *New Journal of Physics* **8**, 15 (2006).
- [4] S. Piano and G. Adesso, Genuine tripartite entanglement and nonlocality in bose-einstein condensates by collective atomic recoil, *Entropy* **15**, 1875 (2013).
- [5] V. Coffman, J. Kundu, and W. K. Wootters, Distributed entanglement, *Phys. Rev. A* **61**, 052306 (2000).
- [6] The residual entanglement between system A and systems B and C is the difference between the entanglement between A and BC jointly, and the sum of the entanglements between A and B and C individually. For pure states, a positive residual entanglement witnesses tripartite entanglement, but it does not faithfully identify all tripartite-entangled states (e.g., the $|W\rangle$ state).
- [7] S. Szalay, Multipartite entanglement measures, *Phys. Rev. A* **92**, 042329 (2015).
- [8] S. Onoe, S. Tserkis, A. P. Lund, and T. C. Ralph, Multipartite gaussian entanglement of formation, *Phys. Rev. A* **102**, 042408 (2020).
- [9] N. Friis, G. Vitagliano, M. Malik, and M. Huber, Entanglement certification from theory to experiment, *Nature Reviews Physics* **1**, 72 (2019).
- [10] P. van Loock and A. Furusawa, Detecting genuine multipartite continuous-variable entanglement, *Phys. Rev. A* **67**, 052315 (2003).
- [11] F. Toscano, A. Saboia, A. T. Avelar, and S. P. Walborn, Systematic construction of genuine-multipartite-entanglement criteria in continuous-variable systems using uncertainty relations, *Phys. Rev. A* **92**, 052316 (2015).
- [12] R. Y. Teh and M. D. Reid, Criteria for genuine n -partite continuous-variable entanglement and einstein-podolsky-rosen steering, *Phys. Rev. A* **90**, 062337 (2014).
- [13] M. Huber, F. Mintert, A. Gabriel, and B. C. Hiesmayr, Detection of high-dimensional genuine multipartite entanglement of mixed states, *Phys. Rev. Lett.* **104**, 210501 (2010).
- [14] M. M. Cunha, A. Fonseca, and E. O. Silva, Tripartite entanglement: Foundations and applications, *Universe* **5**, 10.3390/universe5100209 (2019).
- [15] L. K. Shalm, D. R. Hamel, Z. Yan, C. Simon, K. J. Resch, and T. Jennewein, Three-photon energy-time entanglement, *Nature Physics* **9**, 19 (2013).
- [16] G. Svetlichny, Distinguishing three-body from two-body nonseparability by a bell-type inequality, *Phys. Rev. D* **35**, 3066 (1987).
- [17] J. Schneeloch, C. C. Tison, M. L. Fanto, S. Ray, and P. M. Alsing, Quantifying tripartite entanglement with entropic correlations, *Phys. Rev. Research* **2**, 043152 (2020).
- [18] In [17], it was shown how genuine tripartite entanglement could be quantified in continuous-variable degrees of freedom, but only on the assumption that the joint state was pure.
- [19] B. C. Hiesmayr, M. J. A. de Dood, and W. Löffler, Observation of four-photon orbital angular momentum entanglement, *Phys. Rev. Lett.* **116**, 073601 (2016).
- [20] S. Agne, T. Kauten, J. Jin, E. Meyer-Scott, J. Z. Salvail, D. R. Hamel, K. J. Resch, G. Weihs, and T. Jennewein, Observation of genuine three-photon interference, *Phys. Rev. Lett.* **118**, 153602 (2017).
- [21] S. Krapick, B. Brecht, H. Herrmann, V. Quiring, and C. Silberhorn, On-chip generation of photon-triplet states, *Opt. Express* **24**, 2836 (2016).
- [22] M. G. Moebius, F. Herrera, S. Griesse-Nascimento, O. Reshaf, C. C. Evans, G. G. Guerreschi, A. Aspuru-Guzik, and E. Mazur, Efficient photon triplet generation in integrated nanophotonic waveguides, *Optics express* **24**, 9932 (2016).
- [23] A. T. Avelar and S. P. Walborn, Genuine tripartite continuous-variable entanglement with spatial degrees of freedom of photons, *Phys. Rev. A* **88**, 032308 (2013).
- [24] J. Schneeloch and G. A. Howland, Quantifying high-dimensional entanglement with Einstein-Podolsky-Rosen correlations, *Phys. Rev. A* **97**, 042338 (2018).
- [25] T. M. Cover and J. A. Thomas, *Elements of Information Theory*, 2nd ed. (Wiley and Sons, New York, 2006).
- [26] M. Olsen, Tripartite correlations over two octaves from cascaded harmonic generation, *Optics Communications* **410**, 966 (2018).
- [27] E. R. González, A. Borne, B. Boulanger, J. Levenson, and K. Bencheikh, Continuous-variable triple-photon states quantum entanglement, *Physical review letters* **120**, 043601 (2018).
- [28] J. Schneeloch and J. C. Howell, Introduction to the transverse spatial correlations in spontaneous parametric down-conversion through the biphoton birth zone, *Journal of Optics* **18**, 053501 (2016).
- [29] C. K. Law and J. H. Eberly, Analysis and Interpretation of High Transverse Entanglement in Optical Parametric Down Conversion, *Phys. Rev. Lett.* **92**, 127903 (2004).
- [30] D. R. Hamel, L. K. Shalm, H. Hübel, A. J. Miller, F. Marsili, V. B. Verma, R. P. Mirin, S. W. Nam, K. J. Resch, and T. Jennewein, Direct generation of three-photon polarization entanglement, *Nature Photonics* **8**, 801 (2014).

Appendix A: Proof of position and momentum entropic bounds

In Section II, we gave the following relations for continuous entropy:

$$h(k_A + k_B + k_C) \geq \begin{cases} h(k_A|k_B, k_C) \\ h(k_B|k_A, k_C) \\ h(k_C|k_A, k_B) \end{cases} \quad (\text{A1})$$

and for position, the relation:

$$h\left(x_A - \frac{x_B + x_C}{2}\right) \geq \begin{cases} h(x_A|k_B, x_C) - \log(2) \\ h(x_B|k_A, x_C) - \log(2) \\ h(x_C|k_A, x_B) - \log(2) \end{cases} \quad (\text{A2})$$

To prove these relations, we will use the following five properties of continuous entropy:

(a) The scaling law for continuous entropy:

$$h(ax) = h(x) + \log(|a|) \quad (\text{A3})$$

which also implies: (b) the continuous entropy is constant under reflection:

$$h(x) = h(-x) \quad (\text{A4})$$

(c) Conditioning cannot increase continuous entropy:

$$h(x) \geq h(x|y) \geq h(x|y, z) \geq \dots \quad (\text{A5})$$

(d) Shifting by a conditioned variable cannot change entropy

$$h(x \pm y|y) = h(x|y) \quad (\text{A6})$$

(e) Conditioning on functions of already conditioned variables cannot change the entropy:

$$h(x|y, z) = h(x|y, z, f(y, z)) \quad (\text{A7})$$

To prove the momentum relation (A1), we use property (c):

$$h(k_A + k_B + k_C) \geq \begin{cases} h(k_A + k_B + k_C|k_B, k_C) \\ h(k_A + k_B + k_C|k_A, k_C) \\ h(k_A + k_B + k_C|k_A, k_B) \end{cases} \quad (\text{A8})$$

And then property (d):

$$\begin{aligned} h(k_A + k_B + k_C|k_B, k_C) &= h(k_A|k_B, k_C) \\ h(k_A + k_B + k_C|k_A, k_C) &= h(k_B|k_A, k_C) \\ h(k_A + k_B + k_C|k_A, k_B) &= h(k_C|k_A, k_B) \end{aligned} \quad (\text{A9})$$

To prove the position relation (A2) is less straightforward as the different cases require different sequences of properties.

To obtain the bound for $h(x_A|x_B, x_C)$, we use property (c):

$$h\left(x_A - \frac{x_B + x_C}{2}\right) \geq h\left(x_A - \frac{x_B + x_C}{2} \middle| \frac{x_B + x_C}{2}\right), \quad (\text{A10})$$

and then property (d):

$$h\left(x_A - \frac{x_B + x_C}{2} \middle| \frac{x_B + x_C}{2}\right) = h\left(x_A \middle| \frac{x_B + x_C}{2}\right) \quad (\text{A11})$$

Next, we use property (c):

$$h\left(x_A \middle| \frac{x_B + x_C}{2}\right) \geq h\left(x_A \middle| \frac{x_B + x_C}{2}, x_B, x_C\right) \quad (\text{A12})$$

and finally property (e):

$$h\left(x_A \middle| \frac{x_B + x_C}{2}, x_B, x_C\right) = h(x_A|x_B, x_C) \quad (\text{A13})$$

This bound is further loosened in the interest of symmetry by:

$$h(x_A|x_B, x_C) > h(x_A|x_B, x_C) - \log(2). \quad (\text{A14})$$

To obtain the bounds for $h(x_B|x_A, x_C)$ and $h(x_C|x_A, x_B)$ we start with property (b)

$$\begin{aligned} h\left(x_A - \frac{x_B + x_C}{2}\right) &= h\left(\frac{x_B}{2} - \left(x_A - \frac{x_C}{2}\right)\right) \\ h\left(x_A - \frac{x_B + x_C}{2}\right) &= h\left(\frac{x_C}{2} - \left(x_A - \frac{x_B}{2}\right)\right) \end{aligned} \quad (\text{A15})$$

Then, we use properties (c) and (d)

$$\begin{aligned} h\left(\frac{x_B}{2} - \left(x_A - \frac{x_C}{2}\right)\right) &\geq h\left(\frac{x_B}{2} \middle| x_A - \frac{x_C}{2}\right) \\ h\left(\frac{x_C}{2} - \left(x_A - \frac{x_B}{2}\right)\right) &\geq h\left(\frac{x_C}{2} \middle| x_A - \frac{x_B}{2}\right) \end{aligned} \quad (\text{A16})$$

Next, we use property (c) again:

$$\begin{aligned} h\left(\frac{x_B}{2} \middle| x_A - \frac{x_C}{2}\right) &\geq h\left(\frac{x_B}{2} \middle| x_A - \frac{x_C}{2}, x_A, x_C\right) \\ h\left(\frac{x_C}{2} \middle| x_A - \frac{x_B}{2}\right) &\geq h\left(\frac{x_C}{2} \middle| x_A - \frac{x_B}{2}, x_A, x_B\right) \end{aligned} \quad (\text{A17})$$

followed by property (e):

$$\begin{aligned} h\left(\frac{x_B}{2} \middle| x_A - \frac{x_C}{2}, x_A, x_C\right) &= h\left(\frac{x_B}{2} \middle| x_A, x_C\right) \\ h\left(\frac{x_C}{2} \middle| x_A - \frac{x_B}{2}, x_A, x_B\right) &= h\left(\frac{x_C}{2} \middle| x_A, x_B\right) \end{aligned} \quad (\text{A18})$$

and finally, we use property (a) to finish the bound:

$$\begin{aligned} h\left(\frac{x_B}{2} \middle| x_A, x_C\right) &= h(x_B|x_A, x_C) - \log(2) \\ h\left(\frac{x_C}{2} \middle| x_A, x_B\right) &= h(x_C|x_A, x_B) - \log(2) \end{aligned} \quad (\text{A19})$$

Appendix B: Derivation of triphoton wavefunction for cascaded SPDC

In this section, we show how to derive the triphoton spatial wavefunction in cascaded SPDC. To begin, we have the Hamiltonian for the SPDC process:

$$\hat{H}_{SPDC} = \sum_{k_p, k_1, k_2} G_{k_p, k_1, k_2} \hat{a}_{k_p} \hat{a}_{k_1}^\dagger \hat{a}_{k_2}^\dagger + h.c. \quad (B1)$$

To describe the cascaded SPDC process, we use first-order time-dependent perturbation theory to describe the evolution of the field after interacting with each crystal. After the first interaction ($k_p \rightarrow k_1 + k_2$), and after the second interaction, ($k_2 \rightarrow k_3 + k_4$). The approximate state of the down-converted field after these interactions is:

$$|\psi\rangle_{field} \approx \left(\mathbf{I} + \sum_{k_2, k_3, k_4} G_{k_2, k_3, k_4} \hat{a}_{k_2} \hat{a}_{k_3}^\dagger \hat{a}_{k_4}^\dagger \right) \cdot \left(\mathbf{I} + \sum_{k_p, k_1, k_2} G_{k_p, k_1, k_2} \hat{a}_{k_p} \hat{a}_{k_1}^\dagger \hat{a}_{k_2}^\dagger \right) |vac\rangle \quad (B2)$$

To first non-trivial order in the generation of photon triplets, the state of the photon triplets is described by:

$$|\psi\rangle_{CDC} \approx \sum_{\substack{k_2, k_3, k_4 \\ k_p, k_1, k_2}} G_{k_2, k_3, k_4} G_{k_p, k_1, k_2} \hat{a}_{k_2} \hat{a}_{k_3}^\dagger \hat{a}_{k_4}^\dagger \hat{a}_{k_p} \hat{a}_{k_1}^\dagger \hat{a}_{k_2}^\dagger |vac\rangle \\ = \left(\sum_{k_p, k_1, k_3, k_4} \left(\sum_{k_2} G_{k_2, k_3, k_4} G_{k_p, k_1, k_2} \right) \hat{a}_{k_p} \hat{a}_{k_1}^\dagger \hat{a}_{k_3}^\dagger \hat{a}_{k_4}^\dagger \right) |vac\rangle \quad (B3)$$

where the simplification is carried out by the identity:

$$\hat{a}_{k_2} \hat{a}_{k_2}^\dagger = \hat{a}_{k_2}^\dagger \hat{a}_{k_2} + \delta_{k_2, k_2'} \quad (B4)$$

In [28], the spatially varying components of G_{k_p, k_1, k_2} is given by:

$$G_{k_p, k_1, k_2} \propto \alpha_{k_p} \int d^3r (\chi_{eff}^{(2)}(\vec{r}) e^{-i\vec{\Delta}k \cdot \vec{r}}) \quad (B5)$$

where $\chi_{eff}^{(2)}(\vec{r})$ is the spatially varying second order non-linear susceptibility taken to be a constant inside the non-linear medium unless performing quasi phase matching by periodic poling in which case it flips sign with the flipping poling. Then, for a rectangular crystal of length L_z (and other dimensions L_x and L_y), this integrates to:

$$G_{k_p, k_1, k_2} = \mathcal{N} \alpha_{k_p} \prod_{i=x, y, z} \text{sinc} \left(\frac{\Delta k_i L_i}{2} \right) \quad (B6)$$

$$\Delta k_i = k_{1i} + k_{2i} - k_{pi} - k_{\Lambda i} \quad (B7)$$

$$(B8)$$

where \mathcal{N} is a normalization constant, $k_{\Lambda i}$ is the i -th component of the poling momentum $2\pi/\Lambda$, and Λ is the poling period. In the bulk crystal case without periodic poling, $k_{\Lambda} = 0$.

With the approximate expression for G_{k_p, k_1, k_2} , and assuming the pump is bright enough to replace its annihilation operator with the corresponding coherent state amplitude, we can express the state of the cascaded down-converted light in terms of a triphoton amplitude:

$$|\psi\rangle_{CDC} \approx \sum_{k_1 k_3 k_4} \Psi(\vec{k}_1, \vec{k}_3, \vec{k}_4) \hat{a}_{k_1}^\dagger \hat{a}_{k_3}^\dagger \hat{a}_{k_4}^\dagger |vac\rangle \quad (B9)$$

where

$$\Psi(\vec{k}_1, \vec{k}_3, \vec{k}_4) = \sum_{k_p} \alpha_{k_p} \left(\sum_{k_2} G_{k_2, k_3, k_4} G_{k_p, k_1, k_2} \right) \quad (B10)$$

With the approximate expression for G_{k_p, k_1, k_2} , we approximate the sums in the triphoton amplitude as integrals and note the following simplifications. We assume the pump is sufficiently narrowband in frequency that its longitudinal momentum takes on one value in this sum. Next, we assume the transverse crystal dimensions L_x and L_y are large enough to wholly encompass the beam without clipping any side, which in turn is much larger than the pump wavelength. The transverse sinc functions can only contribute significantly for values less than the order of $2\pi/L_x$ or $2\pi/L_y$, which is multiple orders of magnitude smaller than the pump momentum $2\pi/\lambda_p$. Because of this, they can be treated as delta functions when integrating over the transverse components of the pump momentum. In addition, this enforces transverse momentum conservation.

$$\Psi(\vec{k}_1, \vec{k}_3, \vec{k}_4) \approx \alpha_p (\vec{k}_1 + \vec{k}_3 + \vec{k}_4) \cdot \int dk_{2z} \left(\text{sinc} \left(\frac{(k_{1z} + k_{2z} - k_{pz} - k_{\Lambda 1z})L_z}{2} \right) \cdot \text{sinc} \left(\frac{(k_{3z} + k_{4z} - k_{2z} - k_{\Lambda 2z})L_z}{2} \right) \right) \quad (B11)$$

Here, we are assuming that cascaded SPDC is achieved either simultaneously in the same crystal using two different poling momenta Λ_1 and Λ_2 , or using a sequence of two identical crystals both of length L_z for simplicity. This integral has the form of a convolution, and can be solved to give:

$$\Psi(\vec{k}_1, \vec{k}_3, \vec{k}_4) \approx \alpha_p (\vec{k}_1 + \vec{k}_3 + \vec{k}_4) \cdot \text{sinc} \left(\frac{(k_{3z} + k_{4z} + k_{1z} - k_{pz} - k_{\Lambda 1z} - k_{\Lambda 2z})L_z}{2} \right) \quad (B12)$$

In the small angle approximation, we may factor this triphoton wavefunction out into a transverse wavefunction multiplied by a longitudinal wavefunction, where the transverse wavefunction contains the information about

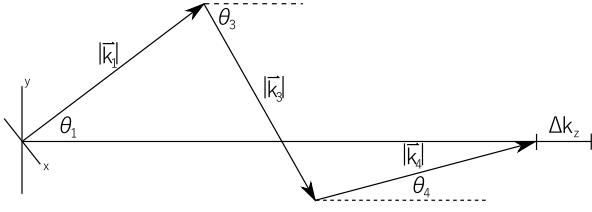


FIG. 4: Basic diagram of phase matched photon triplets generated in cascaded SPDC to obtain the transverse spatial dependence of the phase matching function.

the spatial properties of the down-converted light we would like to measure. To that end, the phase-matching sinc function can be expressed in terms of the transverse momentum components of the photon triplet.

For our triphoton wavefunction, we are considering degenerate collinear photon triplets generated from cascaded SPDC. See Fig. 4 for diagram. These photon triplets have magnitudes $|\vec{k}_1| = |\vec{k}_3| = |\vec{k}_4| = (k_p + k_{\Lambda_1} + k_{\Lambda_2})/3$. Using the small angle approximation, we have:

$$\theta_1 \approx \frac{|\vec{q}_1|}{k_1} = \frac{|\vec{q}_3 + \vec{q}_4|}{k_1} = \frac{3}{k_p} |\vec{q}_3 + \vec{q}_4| \quad (\text{B13})$$

$$\theta_2 \approx \frac{|\vec{q}_2|}{k_2} = \frac{|\vec{q}_1 + \vec{q}_3|}{k_2} = \frac{3}{k_p} |\vec{q}_1 + \vec{q}_3| \quad (\text{B14})$$

$$\theta_3 \approx \frac{|\vec{q}_3|}{k_3} = \frac{|\vec{q}_1 + \vec{q}_4|}{k_3} = \frac{3}{k_p} |\vec{q}_1 + \vec{q}_4| \quad (\text{B15})$$

where $\vec{q}_1 = \vec{k}_1 - k_{1z}\hat{z}$ is the transverse component of \vec{k}_1 , and we have used transverse momentum conservation to set $\vec{q}_1 + \vec{q}_3 + \vec{q}_4 = \vec{q}_p \approx 0$. Then for the longitudinal components, we have the momentum difference in the sinc function:

$$|k_1| \cos(\theta_1) + |k_3| \cos(\theta_3) + |k_4| \cos(\theta_4) - k_p - k_{\Lambda_1} - k_{\Lambda_2} \quad (\text{B16})$$

With the assumption of collinear SPDC, we have that

$$|k_1| + |k_3| + |k_4| - k_p - k_{\Lambda_1} - k_{\Lambda_2} \approx 0 \quad (\text{B17})$$

so that the small-angle approximation for the momentum difference reduces to:

$$-\frac{|k_1|}{2}(\theta_1^2 + \theta_3^2 + \theta_4^2) \quad (\text{B18})$$

which when substituting our relation for the transverse components of momentum gives us the final form of the phase-matching function:

$$\text{sinc} \left(\frac{L_z}{4|k_1|} (|\vec{q}_3 + \vec{q}_4|^2 + |\vec{q}_1 + \vec{q}_4|^2 + |\vec{q}_1 + \vec{q}_3|^2) \right) \quad (\text{B19})$$

If we invoke the assumption that $|k_1| = k_p/3$ such as when using two unpoled bulk crystals where phase matching is achieved by other means (e.g., different materials), and add the pump-dependent portion of the

triphoton wavefunction, we obtain the identical phase-matching function discussed in the body of the paper:

$$\psi(\vec{q}_1, \vec{q}_3, \vec{q}_4) = \mathcal{N} \alpha_p (\vec{q}_1 + \vec{q}_3 + \vec{q}_4) \cdot \text{sinc} \left(\frac{L_z}{4|k_1|} (|\vec{q}_3 + \vec{q}_4|^2 + |\vec{q}_1 + \vec{q}_4|^2 + |\vec{q}_1 + \vec{q}_3|^2) \right) \quad (\text{B20})$$

Appendix C: Exact tripartite entanglement and Schmidt decomposition of triple Gaussian wavefunction

In this appendix, we describe how to find the marginal eigenvalues of system A of tri-partite system ABC described by the triple-Gaussian wavefunction, as well as its exact Schmidt decomposition.

The Double-Gaussian wavefunction $\psi(x_A, x_B)$ is given by:

$$\psi(x_A, x_B) = \frac{1}{\sqrt{2\pi\sigma_+\sigma_-}} e^{-\frac{(x_A+x_B)^2}{8\sigma_+^2}} e^{-\frac{(x_A-x_B)^2}{8\sigma_-^2}} \quad (\text{C1})$$

This wavefunction has the following Schmidt decomposition:

$$\psi(x_A, x_B) = \sum_{n=0}^{\infty} \sqrt{\lambda_n} \phi_n(x_A) \theta_n(x_B) \quad (\text{C2})$$

where

$$\lambda_n = \frac{4r}{(r+1)^2} \left(\frac{r-1}{r+1} \right)^{2n}; \quad (\text{C3})$$

r is the ratio of $\sigma(x_A + x_B)/\sigma(x_A - x_B)$ which simplifies to σ_+/σ_- , and $\phi_n(x)$ is the n th-order Hermite-Gaussian wavefunction as seen in the solutions to the quantum harmonic oscillator. For the double-Gaussian wavefunction, $\theta_n(x) = \phi_n(x)$, though for arbitrary wavefunctions, they can be different.

If we take the marginal density operator of the double-Gaussian state, we find that:

$$\hat{\rho}_A = \int dx_A dx'_A \eta(x_A, x'_A) |x_A\rangle \langle x'_A| \quad (\text{C4})$$

where

$$\eta(x_A, x'_A) = \sum_n \lambda_n \phi_n(x_A) \phi_n(x'_A) \quad (\text{C5})$$

What is important to note are two points. First is that the Schmidt eigenvalues λ_n are geometrically distributed, and second, that the ratio between successive Schmidt coefficients $\sqrt{\lambda_n}$ is given by:

$$\frac{\sqrt{\lambda_{n+1}}}{\sqrt{\lambda_n}} = \frac{r-1}{r+1}. \quad (\text{C6})$$

1. The reduced density operator for the triple-Gaussian wavefunction

The Triple-Gaussian state $|\psi\rangle_{ABC}$ is given by:

$$|\psi\rangle_{ABC} = \int dx_A dx_B dx_C |x_A, x_B, x_C\rangle \langle x_A, x_B, x_C | \psi \rangle_{ABC} \quad (C7)$$

$$= \int dx_A dx_B dx_C |x_A, x_B, x_C\rangle \psi(x_A, x_B, x_C) \quad (C8)$$

where $\psi(x_A, x_B, x_C)$ is the triple-Gaussian wavefunction.

$$\psi(x_A, x_B, x_C) = \frac{e^{-\frac{(x_A+x_B+x_C)^2}{12\sigma_u^2} - \frac{(x_A - \frac{x_B+x_C}{2})^2}{6\sigma_v^2} - \frac{(x_B-x_C)^2}{8\sigma_w^2}}}{\sqrt{(2\pi)^{3/2} \sigma_u \sigma_v \sigma_w}} \quad (C9)$$

where σ_w is set equal to σ_v for rotational symmetry around the x_u -axis.

The density matrix $\hat{\rho}_{ABC}$ corresponding to this state is $|\psi\rangle_{ABC} \langle \psi|_{ABC}$:

$$\hat{\rho}_{ABC} = \int dx_A dx'_A dx_B dx'_B dx_C dx'_C \cdot |x_A, x_B, x_C\rangle \langle x'_A, x'_B, x'_C| \cdot \psi(x_A, x_B, x_C) \psi^*(x'_A, x'_B, x'_C) \quad (C10)$$

Next, we obtain $\hat{\rho}_A$ by tracing over B and C so that we may later obtain the marginal eigenvalues:

$$\hat{\rho}_A = \text{Tr}_{BC}[\hat{\rho}_{ABC}] \quad (C11)$$

$$= \int d\mu_B d\mu_C \langle \mu_B, \mu_C | \hat{\rho}_{ABC} | \mu_B, \mu_C \rangle \quad (C12)$$

$$= \int dx_A dx'_A |x_A\rangle \langle x'_A| \eta(x_A, x'_A) \quad (C13)$$

where

$$\eta(x_A, x'_A) = \int d\mu_B d\mu_C \psi(x_A, \mu_B, \mu_C) \psi^*(x'_A, \mu_B, \mu_C) \quad (C14)$$

Here, $\eta(x_A, x'_A)$ is the density operator function describing $\hat{\rho}_A$.

Now, for the triple-Gaussian wavefunction, $\eta(x_A, x'_A)$ has a Double-Gaussian form:

$$\eta(x_A, x'_A) = \sqrt{\frac{3}{2\pi(\sigma_u^2 + 2\sigma_v^2)}} e^{-\frac{(x_A-x'_A)^2}{24} \left(\frac{1}{\sigma_u^2} + \frac{2}{\sigma_v^2}\right)} \cdot e^{-\frac{9(x_A+x'_A)^2}{24} \left(\frac{1}{\sigma_u^2 + 2\sigma_v^2}\right)} \quad (C15)$$

Since this function is up to a normalization constant, equal to a double-Gaussian wavefunction, we can define its correlation ratio R as $\sigma(x_A + x'_A)/\sigma(x_A - x'_A)$, and obtain the result:

$$R = \frac{1}{3} \sqrt{5 + \frac{2\sigma_u^4 + 2\sigma_v^4}{\sigma_u^2 \sigma_v^2}} \quad (C16)$$

2. Determining marginal eigenvalues through analogy

Importantly, $\eta(x_A, x'_A)$ admits precisely the same type of Schmidt decomposition as the double-Gaussian wavefunction:

$$\eta(x_A, x'_A) = \sum_{n=0}^{\infty} G \sqrt{\nu_n} \phi_n(x_A) \theta_n(x'_A) \quad (C17)$$

where G is a normalization constant. Here again, $\theta_n(x) = \phi_n(x)$.

Because of this, $\eta(x_A, x'_A)$ for the triple-Gaussian, is mathematically identical to $\eta(x_A, x'_A)$ for the double-Gaussian. In particular, we deduce that the eigenvalues of $\hat{\rho}_A$ are given by:

$$\lambda_n = G \sqrt{\nu_n} \quad (C18)$$

Then, the ratio of successive Schmidt coefficients is given by:

$$\frac{\sqrt{\nu_{n+1}}}{\sqrt{\nu_n}} = \frac{\lambda_{n+1}}{\lambda_n} = \frac{R-1}{R+1} \quad (C19)$$

With this set of ratios, we can normalize and find the total list of marginal eigenvalues of $\hat{\rho}_A$:

$$\lambda_n = \frac{2}{1+R} \left(\frac{R-1}{R+1} \right)^n \quad (C20)$$

where R is given in (C16).

With this eigenvalue distribution (i.e., the geometric distribution) the von neumann entropy $S(A)$ has the simple form:

$$S(A) = \frac{h_2(\lambda_0)}{\lambda_0} \quad (C21)$$

where $h_2(\lambda)$ is the binary entropy function:

$$h_2(\lambda) = -\lambda \log_2(\lambda) - (1-\lambda) \log_2(1-\lambda). \quad (C22)$$

Due to the triple Gaussian wavefunction referring to a pure state, and one that is symmetric between parties, this von neumann entropy is also equal to the tripartite entanglement of formation of this state.

a. On the Schmidt decomposition of triphoton wavefunction:

With the marginal eigenvalues of the triple-Gaussian wavefunction known, it is tempting to alledge that one can Schmidt-decompose this wavefunction into a series of triplets of Hermite-Gaussian modes, similar to the case for the double-Gaussian wavefunction:

$$\psi(x_A, x_B, x_C) \neq \sum_n \sqrt{\lambda_n} \phi_n(x_A) \phi_n(x_B) \phi_n(x_C) \quad (C23)$$

This decomposition is not valid because the triple-Gaussian wavefunction for $x_C = 0$ reduces to a double-Gaussian wavefunction, but the alleged decomposition cannot because $\phi_n(0)$ is not a geometric series in n .

However, we find that the true Schmidt decomposition of $\psi(x_A, x_B, x_C)$ (for a bipartite split, e.g., $A \otimes BC$) still involves Hermite-Gaussian wavefunctions, and is of the following form:

$$\psi(x_A, x_B, x_C) = \sum_n \sqrt{\lambda_n} \phi_n(x_A) \theta_n(x_B, x_C) \quad (\text{C24})$$

where $\phi_n(x_A)$ is the n -th order Hermite-Gaussian wavefunction:

$$\phi_n(x_A) = \frac{1}{(2\pi\sigma_A^2)^{1/4}} \frac{1}{\sqrt{n!2^n}} H_n\left(\frac{x}{\sigma_A\sqrt{2}}\right) e^{-\frac{x^2}{4\sigma_A^2}} \quad (\text{C25})$$

where $H_n(x)$ is the n -th order Hermite polynomial of x , and σ_A is given as:

$$\sigma_A = \sqrt{\sigma_u\sigma_v} \left(\frac{\sigma_u^2 + 2\sigma_v^2}{2\sigma_u^2 + \sigma_v^2} \right)^{1/4} \quad (\text{C26})$$

σ_A is not to be confused with $\sigma(x_A)$, the standard deviation of the marginal position, which is $\sqrt{(\sigma_u^2 + 2\sigma_v^2)/3}$.

In this decomposition, $\theta_n(x_B, x_C)$ is an n -th order polynomial double-Gaussian wavefunction, defined here as the product of a Gaussian wavefunction in the rotated coordinate $(x_B - x_C)$ and an n -th order polynomial Gaussian wavefunction in the orthogonal coordinate $(x_B + x_C)$. The explicit form is given by the integral:

$$\sqrt{\lambda_n} \theta_n(x_B, x_C) = \int dx_A \phi_n^*(x_A) \psi(x_A, x_B, x_C) \quad (\text{C27})$$

and $\theta_n(x_B, x_C)$ is determined through renormalization. From this, we were able to determine σ_A (C26), because only the correct value of σ_A would yield the right eigenvalue spectrum λ_n matching with what we obtained with our previous analogy method (C20).

To simplify the integral, $\psi(x_A, x_B, x_C)$ can be re-expressed as:

$$\psi(x_A, x_B, x_C) = \frac{e^{-\frac{(x_A + \sqrt{2}x_p)^2}{12\sigma_u^2} - \frac{(x_A - \frac{x_p}{\sqrt{2}})^2}{6\sigma_v^2} - \frac{x_m^2}{4\sigma_v^2}}}{\sqrt{(2\pi)^{3/2} \sigma_u \sigma_v^2}} \quad (\text{C28})$$

such that:

$$x_p = \frac{x_B + x_C}{\sqrt{2}} \quad : \quad x_m = \frac{x_B - x_C}{\sqrt{2}} \quad (\text{C29})$$

Then, because $\psi(x_A, x_B, x_C)$ factors into a product of a function $g(x_A, x_p)$ and a Gaussian $f(x_m)$, the integral simplifies:

$$\sqrt{\lambda_n} \theta_n(x_B, x_C) = f(x_m) \int dx_A \phi_n^*(x_A) g(x_A, x_p) \quad (\text{C30})$$

Similar to Hermite-Gaussian wavefunctions, this simplified integral is equal to a constant (over order n) Gaussian wavefunction of x_p times an n -th order polynomial of x_p . The form is not recognized by us, so we leave it as an open problem for the interested reader.

Let $\sigma_u = \gamma\sigma_v$; let $s = (\gamma^2 - 1)x_p\sigma_A$; and let $u = (1 + 2\gamma^2\sigma_A^4 - 9\gamma^4\sigma_v^4)$. Then we find:

$$\begin{aligned} & ((1 + 2\gamma^2)\sigma_A^2 + 3\gamma^2\sigma_v^2)^{(n+1/2)} \left(\frac{(2\pi)^{(1/4)}}{2} \right) \cdot \\ & \cdot \int dx_A g(x_A, x_p) \phi_n(x_A) = \\ & = e^{-x_p^2 \left(\frac{3\sigma_A^2 + (2+\gamma^2)\sigma_v^2}{(1+2\gamma^2)\sigma_A^2 + 3\gamma^2\sigma_v^2} \right)} P_n(s, u) \end{aligned} \quad (\text{C31})$$

where up to order $n = 7$ we have:

$$\begin{aligned} P_0 &= \sqrt{6} \\ P_1 &= 2\sqrt{3}s \\ P_2 &= \sqrt{3}(2s^2 - u) \\ P_3 &= \sqrt{2}s(2s^2 - 3u) \\ P_4 &= \frac{1}{2}(4s^4 - 12s^2u + 3u^2) \\ P_5 &= \frac{s}{\sqrt{10}}(4s^4 - 20s^2u + 15u^2) \\ P_6 &= \frac{1}{2\sqrt{30}}(8s^6 - 60s^4u + 90s^2u^2 - 15u^3) \\ P_7 &= \frac{s}{2\sqrt{105}}(8s^6 - 84s^4u + 210s^2u^2 - 105u^3) \end{aligned} \quad (\text{C32})$$